Optical and Quantum Electronics **21** *(1989) 253–282*

TUTORIAL REVIEW

Optical methods for precision measurements

H. J. TIZIANI
University of Stuttgart, Institut für Technische Optik, Pfaffenwaldring 9, 7000 Stuttgart 80, FRG

AN INVITED PAPER

Received 5 December 1988

Contactless measuring techniques are becoming increasingly important for industrial applications. The use of a laser, solid-state detector arrays and powerful small computers leads to a very efficient fringe analysis in holography as well as in Moiré and speckle techniques. Due to the computer analysis, much more information can be extracted from interferograms, leading to higher sensitivities and accuracies. The application of different fringe analysis procedures is discussed, together with some potentials of the application of interferometry, holography, and speckle and Moiré techniques.

1. Introduction

Interferometry, holography, speckle and Moiré techniques are becoming useful tools for precision measurements in research and for industrial applications. Computer analysis is increasingly important for fringe analysis. The use of solid-state detector arrays, image memory boards together with microprocessors and computers for the extraction of the information from the interferograms and high-resolution graphic boards finds important application in optical metrology. Much more information can be extracted from the interferograms, leading to higher sensitivities and accuracies.

Fringe analysis procedures including fringe peak detection and fringe order determination are tedious and time-consuming. Automatic fringe analysis and precision phase measuring techniques are very important in applying interferometric techniques. Automatic quantitative evaluation of interferograms requires accurate interference phase measurements, independent of fringe position and intensity variations superposed onto the interferograms. In many interferometric arrangements, phase shifting or heterodyne techniques have been introduced for automatic fringe analysis.

In the phase shifting technique or quasi-heterodyne technique the relative phase is changed continuously or stepwise, using at least three phase shifts of 90° or 120°, for instance. The phase of the interference patterns can then be computed from the different measured intensity values. The phase shifting technique is very appropriate for digital processing and TV techniques. Interferometry and two-reference-beam holography together with video electronic processing lead to a sensitivity of 1/100 of a fringe at any point of the fringe pattern in the TV image. In heterodyne methods the relative phase increases linearly

0306–8919/89 $03.00 + .12

in time and the reference phase is measured electronically at the beat frequency of the reconstructed wave-fields. Heterodyne interferometry and holographic interferometry offer high spatial resolution and interpolation up to 1/1000 of a fringe. It requires, however, sophisticated electronic equipment and mechanical scanning of the fringe pattern [1].

For engineering applications it is desirable to have real-time techniques in interferometry and holographic interferometry, as well as for speckle applications. Thermoplastic material is frequently used for hologram storage in engineering applications. Photorefractive crystals are found to be useful for real-time holography and speckle applications. In speckle interferometry, video techniques can be applied to record the speckle pattern. In the following discussion methods are described together with some applications partly from our laboratory.

2. Automatic fringe analysis and phase-measuring interferometry

The introduction of the laser in 1960 and the progress made recently in automatic fringe analysis are mostly responsible for the widespread application of interferometry in industry today. Some methods and applications will be discussed briefly for two-beam interferometry. Fringe analysis will be similar in holography, speckle applications and Moiré techniques. The superposition of the two wavefields $a_1\cos[\omega t - \phi_1(\boldsymbol{x})]$ and $a_2\cos[\omega t - \phi_2(\boldsymbol{x})]$ lead to the intensity

$$I(\boldsymbol{x}) = I_0[1 + m\cos\phi(\boldsymbol{x})] \tag{1}$$

where $\phi(\boldsymbol{x}) = \phi_1(\boldsymbol{x}) - \phi_2(\boldsymbol{x})$, $I_0 = |a_1|^2 + |a_2|^2$ and

$$m = \frac{2|a_1||a_2|}{|a_1|^2 + |a_2|^2}$$

m being the modulation of interference fringes.

The phase ϕ can be determined from the detector signal of an interference arrangement. There are the following problems to be investigated: three unknowns (I_0, m and ϕ); ϕ is determined to a factor of 2π only; and sign ϕ is to be determined. In addition, the accuracy can be drastically increased by an appropriate interpolation technique. Digital interferometry provides the means for obtaining very precise measurements at rapid rates.

For the fringe analysis many different methods are applied. They can be classified into static and dynamic methods [2–10].

3. Fringe analysis with static techniques

For the fringe analysis using static methods a tilt is often introduced to avoid closed fringes. The fringe centres can be found manually and by using a digitizing tablet as well as by using video- and image-processing techniques.

To estimate fringe peaks, the fringe density binarization technique is commonly used in many fringe analysis systems because of the simple algorithms used. The grey-level method, where the local variation of fringe density is considered, is sensitive to noise, but can detect peaks by processing only local areas smaller than those in the binary case. In order to extract fringe peaks in the grey-level method, it is very important to diminish the influence of noise, including speckle noise. A simple and effective way is unweighted averaging.

Carrier fringe analysis in the spatial domain using Fourier techniques can be very useful. The Fourier-transformation technique was first proposed by Takeda *et al.* [2] and extended

by Kreis [3]. Equation 1 can be rewritten as

$$I(x, y) = A(x, y) + B(x, y)\cos[\phi(x, y) + (2\pi/\lambda)x \sin \vartheta] \tag{2}$$

where the bias phase is introduced by a tilt ϑ into an interferometric fringe pattern. Equation 2 can be written as

$$I(f_x, f_y) = A(x, y) + C(x, y)\exp[i(2\pi/\lambda)x \sin \vartheta] + C^*(x, y)\exp[-i(2\pi/\lambda)x \sin \vartheta]$$

where $C(x, y) = \frac{1}{2}B(x, y)\exp[i\phi(x, y)]$ and $C^*(x, y)$ is its complex conjugate. In Fourier domain analysis, the conjugate carrier fringe pattern is Fourier transformed to obtain

$$\tilde{I}(f_x, f_y) = \tilde{A}(f_x, f_y) + \tilde{C}(f_x - f_0, f_y) + \tilde{C}^*(f_x + f_0, f_y)$$

where $\tilde{I}$, $\tilde{A}$, $\tilde{C}$ and $\tilde{C}^*$ are the Fourier transforms of I, A, C and C^*. If the tilt introduced is appropriate, the terms $\tilde{A}$, $\tilde{C}$ and $\tilde{C}^*$ are separated in the Fourier domain. The term $\tilde{C}(f_x - f_0, f_y)$ contains the information of the phase $\phi(x, y)$. Shifting it mathematically to the origin in the Fourier domain gives the term $\tilde{C}(f_x, f_y)$ which, in turn Fourier transformed back, leads to $C(x, y)$. It can be easily seen that the imaginary part of its logarithm leads to the phase $\phi(x, y)$:

$$\ln C(x, y) = \ln[B(x, y)/2] + i\phi(x, y) \tag{3}$$

Fig. 1 shows the procedure of the phase detection in the spatial domain using Fourier transformation. Care needs to be taken when filtering $\tilde{C}(f_x, f_y)$ for cleaning up the fringe pattern not to take away useful information. In Fig. 1a, a fringe pattern with a tilt introduced is shown, whereas Fig. 1b shows the corresponding Fourier transform.

In Fig. 2 a typical fringe analysis using the Fourier-transformation method is demonstrated to compare the surface topography with an almost perfect spherical surface. Fig. 2a shows the digitized fringe pattern of Fig. 1a obtained experimentally in a two-beam interference arrangement (Fizeau) in a pseudo-three-dimensional representation, and Fig. 2b represents the contour lines. The contour lines correspond to height variation of 0.54 μm.

Furthermore, from equation 3, $\phi(x, y)$ can be calculated at each point:

$$\phi(x, y) = \arctan\left(\frac{\operatorname{Im} C(x, y)}{\operatorname{Re} C(x, y)}\right) \tag{4}$$

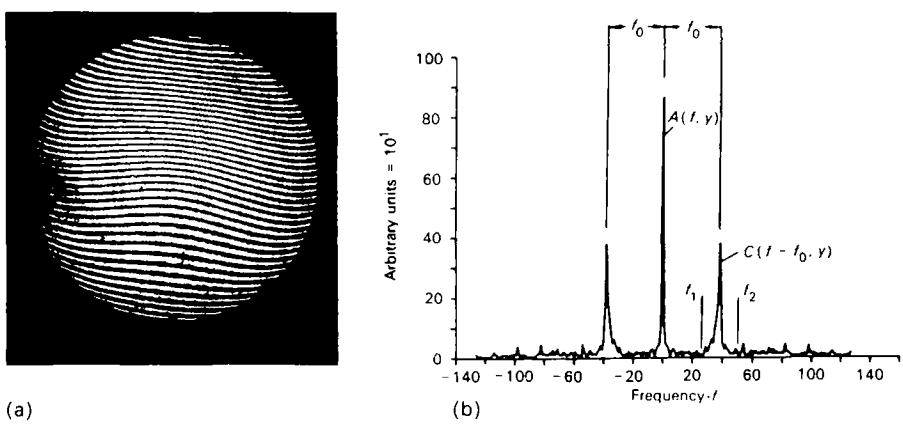

Figure 1 Principle of automatric fringe analysis using the Fourier transform method. (a) Interferogram with tilt and (b) Fourier spectrum.

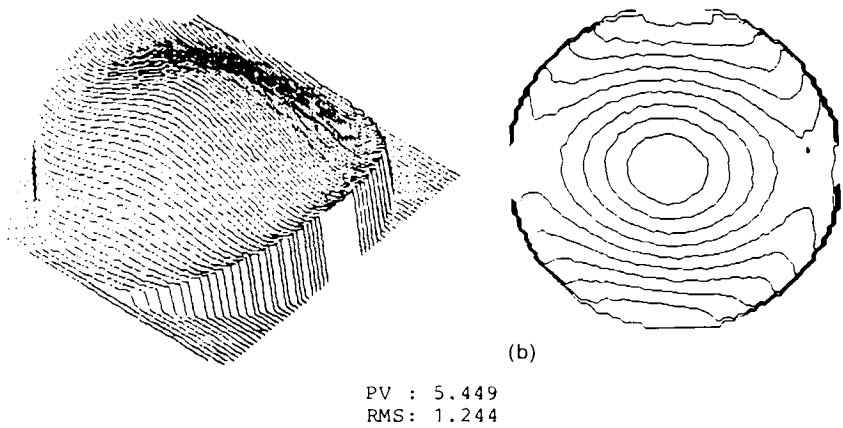

Figure 2 Fringe analysis of the fringe pattern in Fig. 1a with automatic tilt compensation (a) in pseudo-three-dimensional and (b) in contour line representation, where the contour lines correspond to height variations of 0.54 μm.

The signs of the numerator and denominator have to be taken into account separately to obtain values ranging from $-\pi$ to $+\pi$. The ambiguities of 2π can be overcome by complementary information. The sign ambiguity may be overcome by the detection of slope changes; the sign-reversal points can be detected by using two reconstructions with an arbitrary phase shift between them.

The Fourier-transform method usually does not require phase shifts. By a pointwise analysis the determination of phase variations even in sub-wavelength range is obtained from one interferogram. The method can be very valuable in holographic interferometry, and Moiré techniques.

4. Fringe analysis with dynamic techniques

For dynamic algorithms the relative phase between the reference beam and the test beam in an interferometer is varied at a constant, controlled rate or in steps, of 90° or 120° for instance [4–10]. Dynamic techniques are: phase shifting in three, four or more steps, or continuously; the heterodyne technique; and the phase-locked technique.

4.1. Phase-shifting techniques

The intensity of the interference pattern can be written as

$$I_m(x, y) = I_0(x, y)\{1 + m(x, y)\cos[\phi(x, y) + \Delta k]\} \tag{5}$$

where $\phi(x, y) = (2\pi/\lambda)W(x, y)$ is the phase distribution of the wavefront $W(x, y)$ across the interference pattern to be measured and Δ is the deliberately introduced phase shift. $k = 1, 2, 3, \ldots, N$, depending on the number of phase shifts introduced.

The interference pattern can be recorded by a solid-state detector array. For the shifting technique at least three patterns with the appropriate phase shifts need to be recorded [4–10]. Applying the four-phase shift method $(-3\pi/4, -\pi/4, \pi/4, 3\pi/4)$, the phase of the wavefront computed from the four interferograms is

$$\phi(x, y) = \arctan\left(\frac{I_4(x, y) - I_2(x, y)}{I_1(x, y) - I_3(x, y)}\right) \tag{6}$$

For accurate phase analysis, the phase shifts introduced by a piezo-element, for instance, need to be measured for the piezo to be calibrated. An error of $\lambda/10$ in the wavefront occurs by an error in the phase shift of 20%. Care needs to be taken when phase shifts in strongly diverging or converging beams are necessary. Schwider *et al.* [6] proposed a four-step phase shift procedure with an averaging algorithm:

$$\phi(x, y) = \frac{1}{2}\left(\arctan\frac{I_3(x, y) - I_2(x, y)}{I_1(x, y) - I_2(x, y)} + \arctan\frac{I_4(x, y) - I_3(x, y)}{I_2(x, y) - I_3(x, y)}\right) \tag{7}$$

This leads to a reduction of errors introduced by inaccurate phase shifts. Furthermore, the phase stepping could be anything between 0° and 180°. By the integrating bucket technique [7, 8] the intensity of the fringe pattern is integrated in buckets while the phase is being shifted.

For high-accuracy measurements of flat and spherical surfaces it is useful to work with few fringes; a phase calculation algorithm with five measurements of intensity is desirable. The corresponding phase steps are -2Δ, $-\Delta$, 0, Δ and 2Δ. For $\Delta = 90°$

$$\tan\phi = \frac{2(I_2 - I_4)}{2I_3 - I_5 - I_1} \tag{8}$$

The preliminary calibration of the piezo to ensure that the phase step is approximately equal to 90° can be carried out with four out of five values of intensity [6], namely

$$\cos\Delta = \frac{I_5 - I_1}{2(I_4 - I_2)} \tag{9}$$

Because the five-interferogram method is not strongly affected by phase stepping errors, it is particularly interesting in a Fizeau arrangement where, for different aperture heights, different phase shifts occur while shifting the test surface or the reference.

For comparison, examples of fringe analysis of a surface in a Fizeau arrangement are shown in Figs 2 and 3. The fringe analysis of the interferogram in Fig. 3 obtained with a Fizeau arrangement is based on phase shifting with five phase steps. Fig. 3a shows the fringe pattern, Fig. 3b the pseudo-three-dimensional plot and Fig. 3c the contour lines. A very good agreement between the static and dynamic techniques with fringe shifting was obtained. By applying the Fourier-transform method closed fringes should be avoided. Fig. 4 shows schematically the typical hardware used here for fringe analysis.

Digital interferometry is very useful for getting the interferometric data into a computer for the analysis. An experimental arrangement based on a Twyman–Green interferometer is shown in Fig. 5. For the automatic analysis of closed fringes a phase-shift technique is appropriate. Phase shifts can be introduced by tilting a plane-parallel plate, moving a mirror by means of piezo-elements or by polarization techniques. In Fig. 6 a diamond-turned germanium spherical surface is analysed, showing shape errors. In Fig. 6a fringe patterns with different introduced tilts are shown, and Fig. 6b gives the one-dimensional fringe analysis of Fig. 6a with a tilt compensation. The quasi-microroughness analysis obtained by fringe analysis of the same interferogram is shown in Fig. 6c, where the shape is subtracted. The sensitivity obtained is $\lambda/100$.

For microprofile measurements, stylus instruments are among the most highly developed means of profiling precision surfaces. Interferometry with fringe analysis can be used for microstructure analysis. An adapted interference arrangement with high numerical aperture,

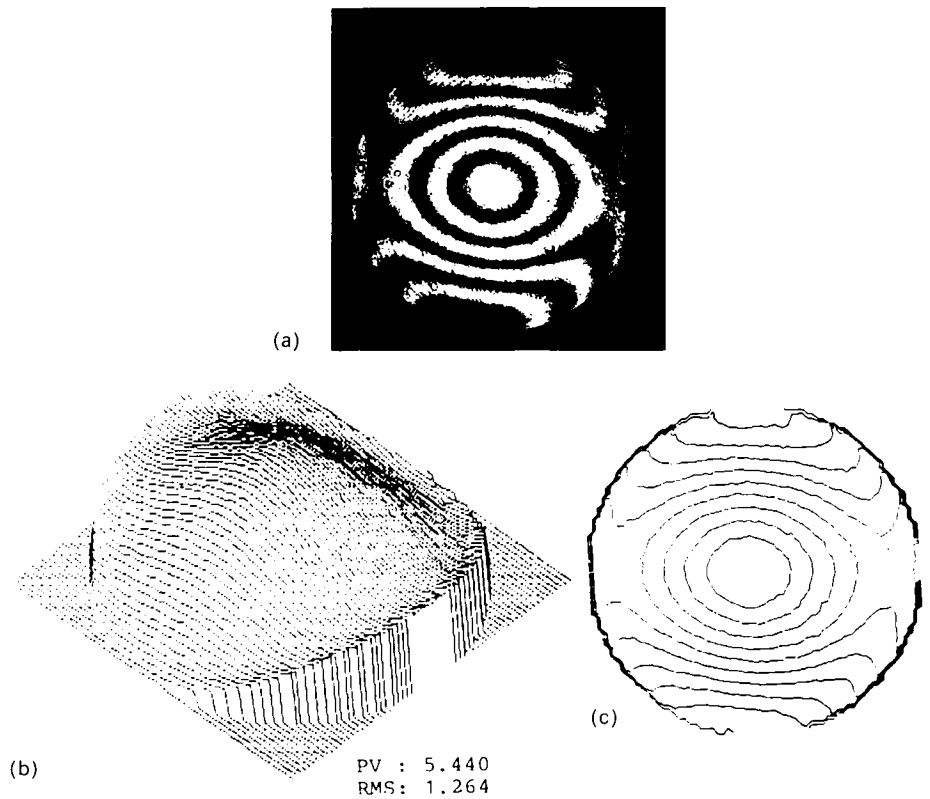

Figure 3 (a) Fringe pattern obtained in a Fizeau arrangement. (b) Fringe pattern analysed using the five-phase-step method in pseudo-three-dimensional representation. (c) Contour line representation of Fig. 3a with contour line separations corresponding to $\Delta h = 0.54\,\mu$m.

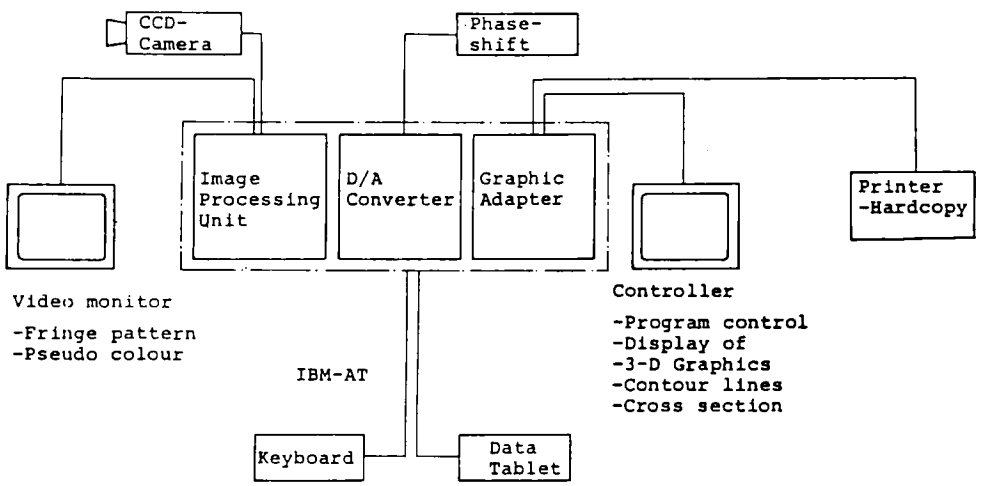

Figure 4 Hardware used for fringe analysis.

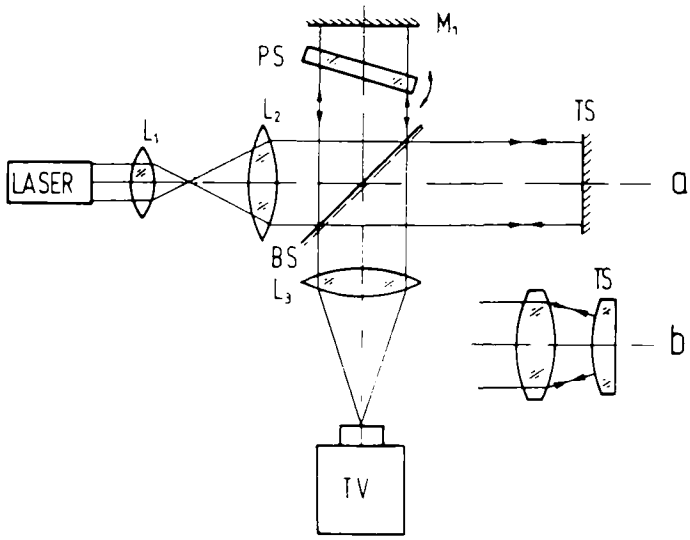

Figure 5 Twyman–Green interferometer. TS, test surfaces; PS, plane-parallel plate to be tilted for phase shifting; BS, beamsplitter; M_1, reference mirror.

NA = 0.9, is shown in Fig. 7b. A piezo-element shifts the phase by displacing the beamsplitter in steps. A diode array of 500 × 580 elements was used to study the compact disc with a pitch of 0.6 μm shown in Fig. 8.

Often it is useful to describe the wavefront by polynomials. Zernike polynomials are preferred because of their orthogonal properties. For special applications Zernike–Tatian polynomials (for a system with a central obstruction) or Tschebyscheff polynomials are useful [9, 11].

4.2. Heterodyne techniques

In interferometry, phase differences of optical fields are transformed into detectable intensity variations. In heterodyne interferometry the time-dependent phase variation is analysed in the frequency space. The two light fields are assumed to be

$$\begin{aligned} A_1 &= a_1 \cos[\omega t + \phi_1(x, y)] \\ A_2 &= a_2 \cos[\omega t + \Delta\omega t + \phi_2(x, y) \pm \phi(x, y, t)] \end{aligned} \tag{10}$$

where $\Delta\omega$ is proportional to the frequency shift $f_2 - f_1$ and $\phi(x, y, t)$ is the time-varying phase shift leading to a frequency shift by interference of the two wavefields:

$$I(x, y) = I_0\{1 + m(x, y)\cos[\Delta\omega t \pm \phi(x, y, t) + \phi_2(x, y) - \phi_1(x, y)]\} \tag{11}$$

from which the time-varying phase $\phi(x, y, t)$ can be detected.

The Doppler shift frequency is

$$\delta f = \frac{\phi(x, y, t)}{2\pi t} = \frac{2}{\lambda}\frac{\mathrm{d}z}{\mathrm{d}t} \tag{12}$$

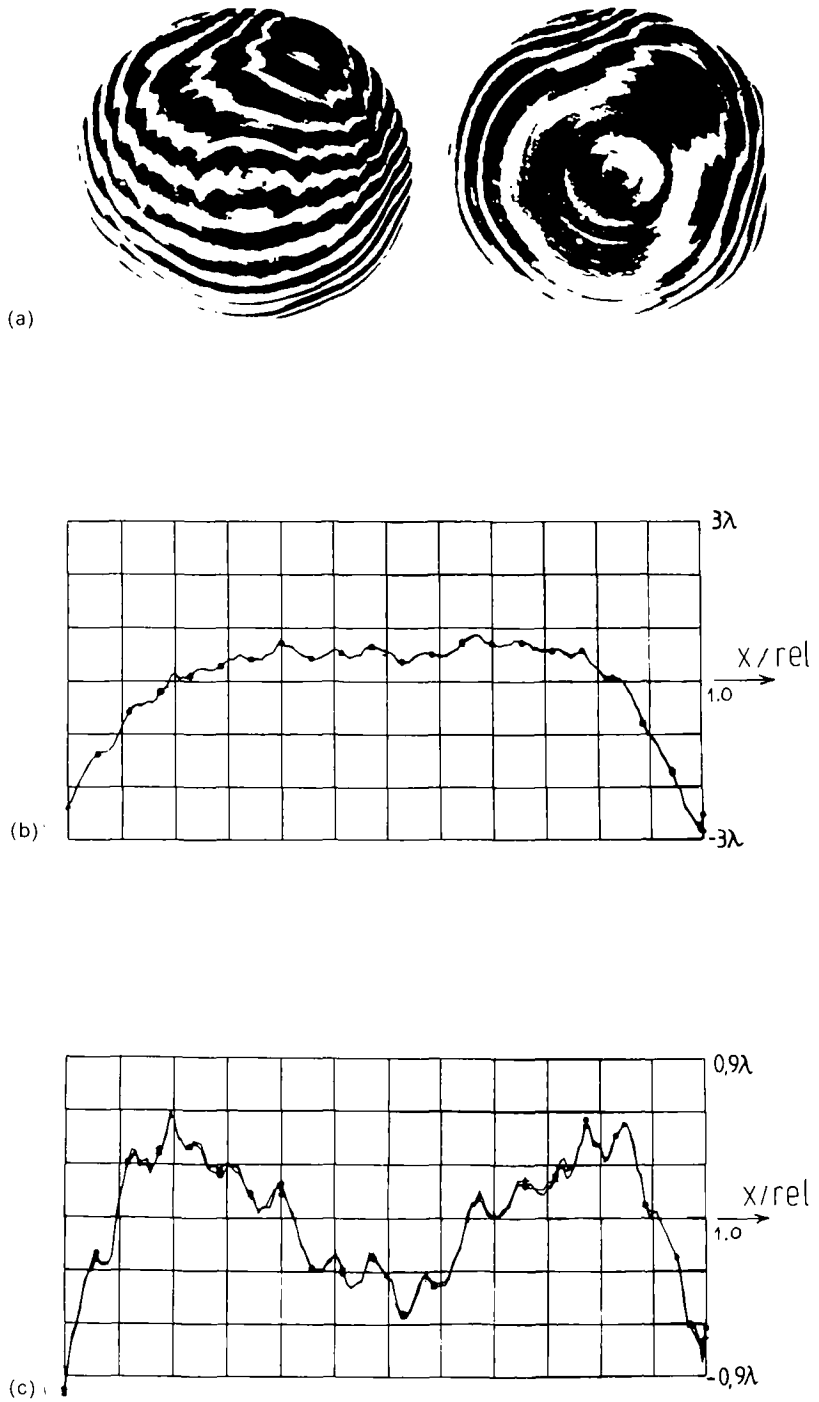

Figure 6 Surface analysis of a diamond-turned germanium surface. (a) Interferograms with different tilts, (b) one-dimensional fringe analysis of (a) with tilt compensation using 2048 data points and (c) microstructure analysis of (a) by subtracting the shape.

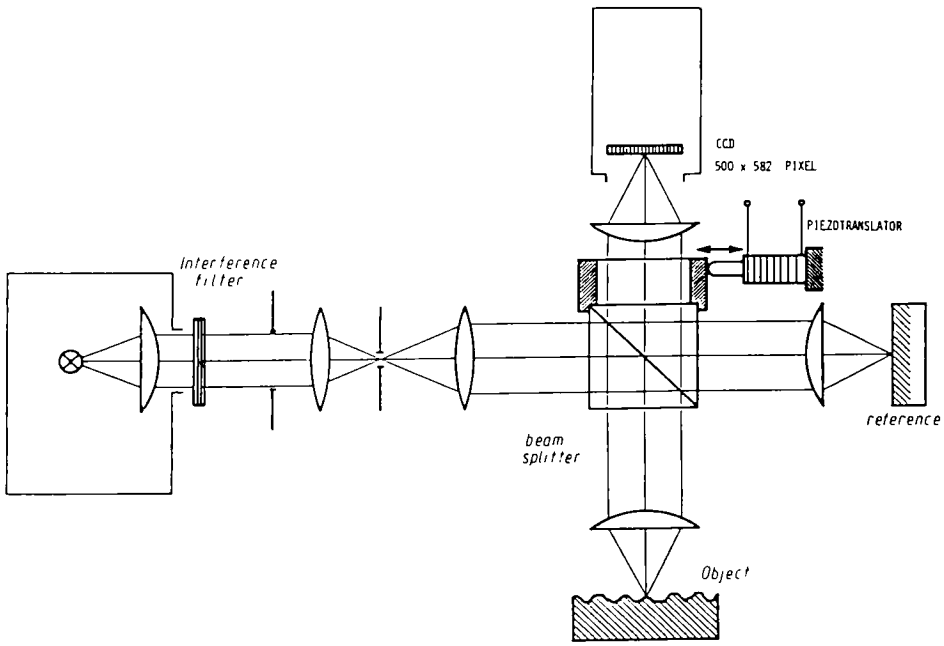

Figure 7 Leitz interference microscope with adapted phase shifting with piezotranslator.

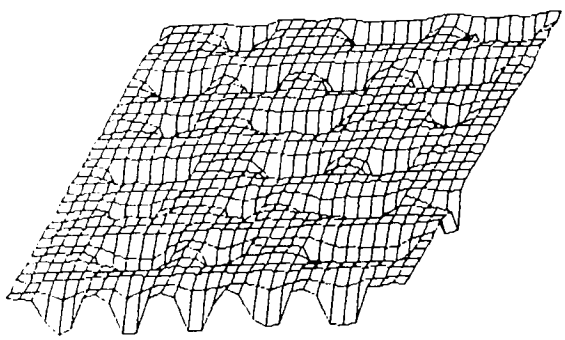

Figure 8 Fringe analysis of a compact disc with a pitch size of 0.6 μm and depth of 120 nm.

where z is the displacement projected parallel to the line of sight

$$z = \frac{\lambda}{2} \int_{t_1}^{t_2} \delta f \, dt$$

This is basically the concept of the well-known interferometer developed by Hewlett-Packard. For a harmonically oscillating object, $\phi(x, y, t) = (4\pi\varrho/\lambda)\cos(\Omega t)$, producing a frequency-modulated output signal at the detector with carrier frequency of $\Delta\omega/2\pi$ and amplitude and frequency of oscillation of ϱ and Ω, respectively. The signal can be evaluated by common frequency analysis techniques [1].

Fig. 9 shows schematicallly a two-beam heterodyne interferometer arrangement we use for microprofile measurement. The two orthogonal polarized beams of frequency f_1 and f_2 are obtained by the magnetic field in the resonator (Zeeman splitting). The difference

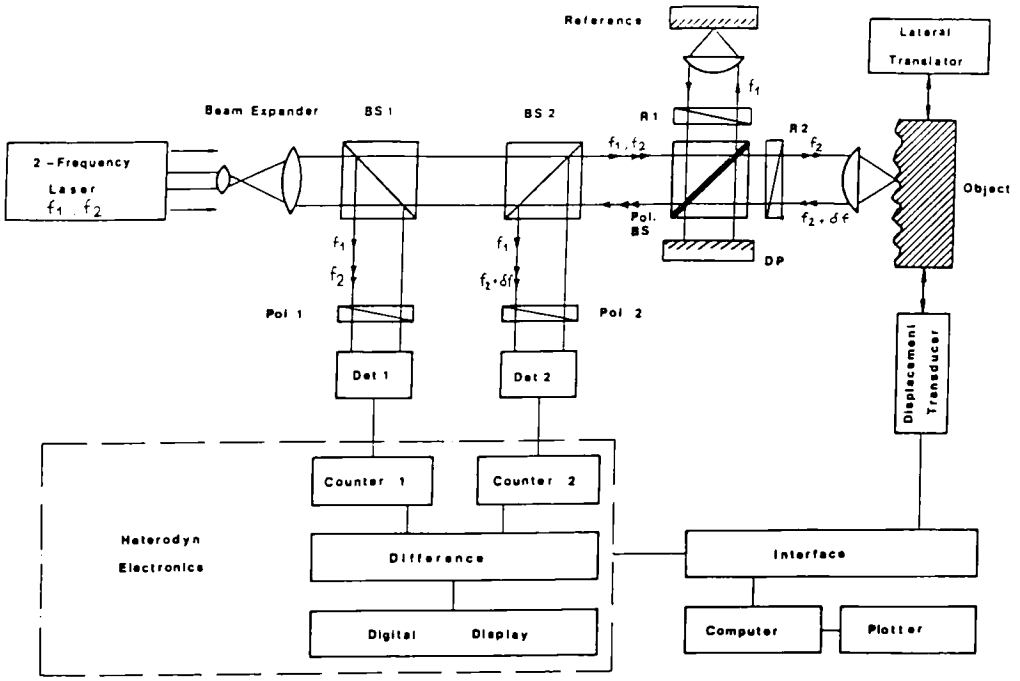

Figure 9 Arrangement for two-beam heterodyne interferometry for microprofile measurement, using a two-frequency laser with frequencies f_1 and f_2 obtained by Zeeman splitting in the laser resonator (f_1 and f_2 are left- and right-hand circularly polarized). The beam separation of the reference with frequency f_1 and object beam with frequency f_2 is obtained by a polarizing beamsplitter, Pol. BS. BS_1 and BS_2 are beamsplitters, R_1 and R_2 are $\lambda/4$ plates. DP is a mirror used for slope compensation.

frequency of 2 MHz is detected by Det 1. The height variation z due to object scanning is recorded by Det 2. A polarizing beamsplitter separates the waves with frequencies f_1 and f_2. The frequency f_2 is modified by the height variation. After passing the quarter-wave plates R_1 and R_2 twice the beams are recombined and finally compared with the instrumental frequency shift. Lenses with high numerical aperture are needed for large slopes of the rough surfaces. For slope compensation a double-pass arrangement is used, as indicated in Fig. 9 by DP.

Fig. 10 shows a typical result obtained. Resolutions of 1 μm laterally and 0.5 nm in depth were obtained by scanning a mirror-like surface. Depth resolutions of 0.1 nm or better were reported by a reduced lateral resolution [12]. Heterodyne techniques are the most promising methods for contactless high-resolution microprofile analysis [12–14]. Other techniques will be developed to be robust for industrial applications with an extended range.

The relationship between the measured heights, determined with different techniques, and the commonly used characterization of surfaces in industry needs to be investigated further. The definition used is given below; new standards may be needed (Section 5).

A similar arrangement to that shown schematically in Fig. 11 was used for the vibration and noise analysis of rotating car tyres. The frequency analysis perpendicular to the surface at a single point of the sidewall is shown in Fig. 12. For comparison the result from an independent measurement obtained with a microphone is indicated by the broken lines in

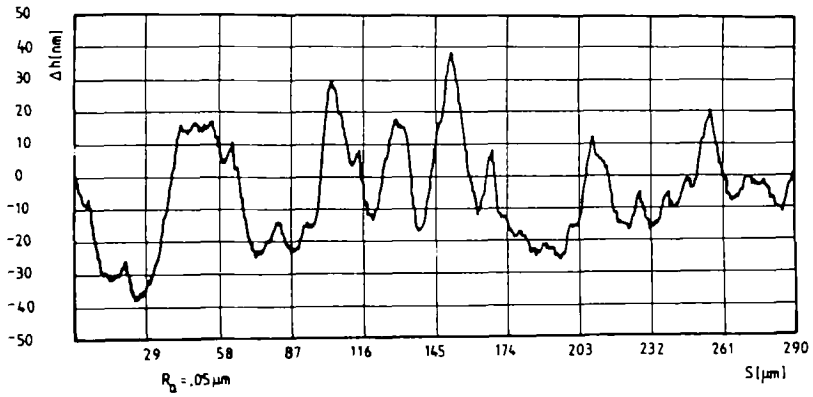

Figure 10 Microprofile of a mirror-like object with a mean roughness R_a = 0.05 μm.

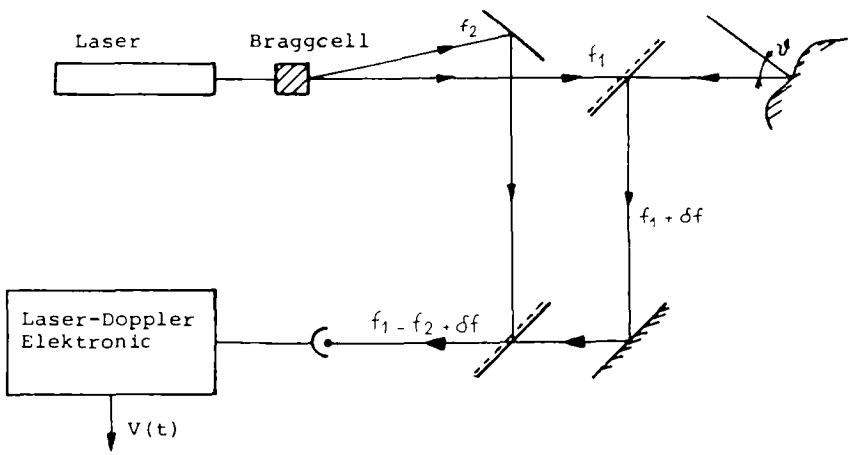

Figure 11 Arrangement for two-beam heterodyne interferometry with a Bragg cell for vibration analysis. The Bragg cell shifts the reference beam with frequency f_2 by 2 MHz, whereas the object beam with frequency f_1 is shifted by the path variation of the object point.

Fig. 12. Close agreement was found between the noise detected with a microphone and the analysis of mechanical vibrations when air-pumping was small [15]. By comparison, a result of double-pulse holography of the rotating car tyre is shown below, in Fig. 20.

Heterodyne interferometry will lead to very useful future applications in precision measurements. For vibration analysis at given points, heterodyne interferometry gives not only the amplitude component of the vibration parallel to the line of sight, but also the frequency. In addition, it can be very useful for fringe analysis in holographic interferometry. It can be used to relate the holographic interference fringes to a known amplitude of variation at a selected point. Furthermore, the heterodyne technique can be extended to speckle interferometry for vibration analysis.

By contrast, the laser Doppler velocimeter is used to measure flow of gases and liquids, using the light scattered from small particles suspended in the flowing medium. The speed of optically rough surfaces can be determined by similar methods.

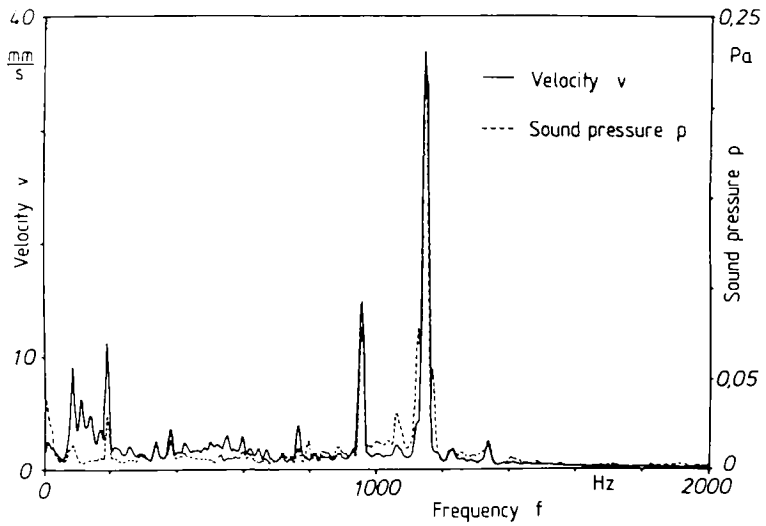

Figure 12 Frequency analysis of a rotating car tyre. The heterodyne interferometer was adapted to the arrangement shown in Fig. 19 with a beam derotator, for instance. For comparison, a microphone was used to measure the noise at the same region. (——) Velocity; (- - -) sound pressure.

Heterodyne interferometry is used for distance measurement as well as for microstructure analysis based on scanning the object point by point. The technique can also be applied for fringe analysis in holographic interferometry [1, 10].

Shearing and two-wavelength techniques are very valuable for testing steep surfaces. Using two-wavelength techniques a variable measurement sensitivity is attainable, with a resultant wavelength larger than the individual. Two-wavelength interferometry can be used for ranging and contouring at reduced sensitivity. Recently, two-wavelength heterodyne interferometry has been reported to be applied for smooth and to some extent for rough surfaces. Because of the availability of multiple-wavelength lasers and tunable diode lasers as light sources, multiple-wavelength interferometry with small wavelength differences is becoming very interesting for practical applications. Using two wavelengths, λ_1 and λ_2, the effective difference wavelength is $\Lambda = \lambda_1\lambda_2/(\lambda_1 - \lambda_2)$ without being obliged to have interferometric stability at the optical wavelengths λ_1 and λ_2 and to separate this wavelength optically. This is of great importance for future range-finding and industrial measurement of distance.

4.3. Phase-locked technique

A phase-locked technique will be discussed in connection with one of our applications for subsurface material analysis. For non-destructive material analysis, photoacoustic and photothermal methods can be applied [16]. In photothermal interferometry the thermal expansion of the specimen is measured rather than the thermal wave itself [17]. Fig. 13 shows an experimental arrangement where a modulated argon-ion laser heats the object under test, leading to a heat wave that propagates through the material and deforms the surface by a few nanometres. An interference arrangement detects the deformation, using a phase-locked technique, where the piezo shifts the phase appropriately. The intensity at the detector of a two-beam interference arrangement can be written according to Fig. 13

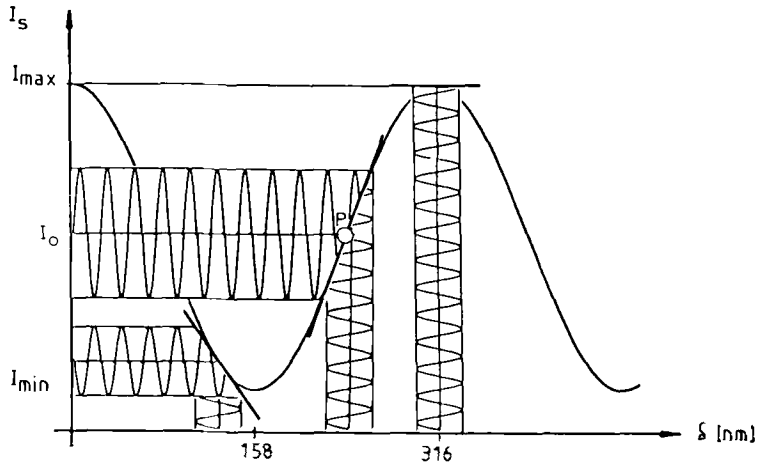

Figure 13 Principle of phase-locked interferometry.

and Equation 1:

$$I_S = I_0(1 + m\cos\phi) \tag{13}$$

where

$$I_0 = (I_{max} + I_{min})/2$$

$$m = \frac{I_{max} - I_{min}}{I_{max} + I_{min}}$$

Here I_{max} and I_{min} are the maximum and the minimum intensity and the phase $\phi = (4\pi/\lambda)W$, where W is the optical path difference. The optical path difference introduced by thermal expansion is a few nanometres only. Care needs to be taken to adjust the interferometer in order to work in the linear region with maximum positive gradient near P in Fig. 13. This is important for maximum sensitivity, and minimum adjustment time and ambiguity of a lock-in amplifier.

$W = W_T + W_r + W_p$ with the thermal expansion W_T, the specimen's surface roughness W_r and the piezo-crystal displacement W_p. W_p is adjusted relative to W_r to work near P in Fig. 13 in order to arrive at a nearly linear relationship between I_S and the path variation W_T due to thermal expansion. λ_s is the wavelength of the interferometer (HeNe).

For a small thermal expansion

$$I_s = I_0[1 + m(2\pi/\lambda_s)W_T]$$

Phase-locked techniques in two-beam arrangements can detect phase differences of $\lambda/100$ and may be used for measuring surface topography and subsurface defects. The interferometer incorporates, as part of a servo-system, a piezoelectrically driven mirror that is capable of applying a known optical phase offset and a periodic optical modulation. The a.c. signal is processed to generate an error signal for the servo-system. A signal proportional to the phase difference between two beams occurs.

A two-beam interferometer using a HeNe laser is shown in Fig. 14 for the analysis of subsurface defects by measuring the small surface deformation caused by a chopped,

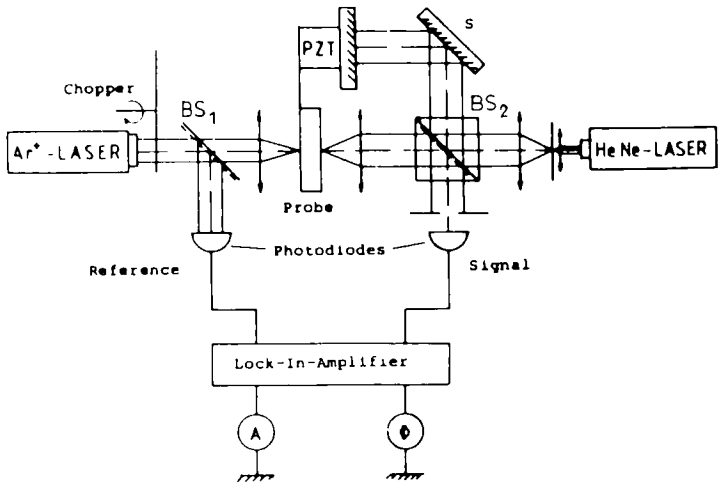

Figure 14 Arrangement for photothermal interferometry in reflection. The probe is heated by an amplitude-modulated argon-ion laser. A piezoelectrically driven mirror, PZT, shifts the phase appropriately in the interference arrangement with the beamsplitter BS_2.

focused argon laser beam with wavelength λ ($\lambda = 488$ nm). The interferometer arrangement is not very sensitive to vibration occurring due to scanning the object. The computer-controlled piezo-element compensates the surface roughness and adjusts the interferometer to work in the linear region with maximum positive gradient. This leads to the maximum sensitivity and minimum adjustment time of the lock-in amplifier. A result is shown in Fig. 15, where a 3 mm thick aluminium plate with holes of diameter 0.8 mm was analysed. The phase measurement indicates clearly the disturbance in the material. The chopper frequency was varied from 20 to 140 Hz. A modified configuration was used to study opaque materials in reflection. Increasing the chopping frequency from a few hundred hertz to a few megahertz leads to very sensitive subsurface defect analysis by a reduced depth range of course.

5. Interferometry for roughness measurements

In the interferometric method described above, applications for surface roughness measurements were indicated. Surface roughness has been measured by stylus instruments where the displacement of a mechanical control element is measured. The surface-contacting element has a radius of a few micrometres and a surface pressure which is not always negligible. Therefore, contactless measuring techniques are desirable.

For roughness measurements the height variation can be represented by the mean roughness R_a or by the root-mean-square roughness R_q or the variance σ_z:

$$R_a = \frac{1}{N}\sum_{i=1}^{N}|Z_i| \qquad R_a = \frac{1}{L}\int_0^L Z(x)\,\mathrm{d}x$$

$$R_q = \left(\frac{1}{N}\sum_{i=1}^{N}Z_i^2\right)^{1/2} \qquad R_q = \left(\frac{1}{L}\int_0^L Z^2(x)\,\mathrm{d}x\right)^{1/2} \tag{14}$$

$$\sigma_z = (E\langle Z_i^2\rangle)^{1/2}$$

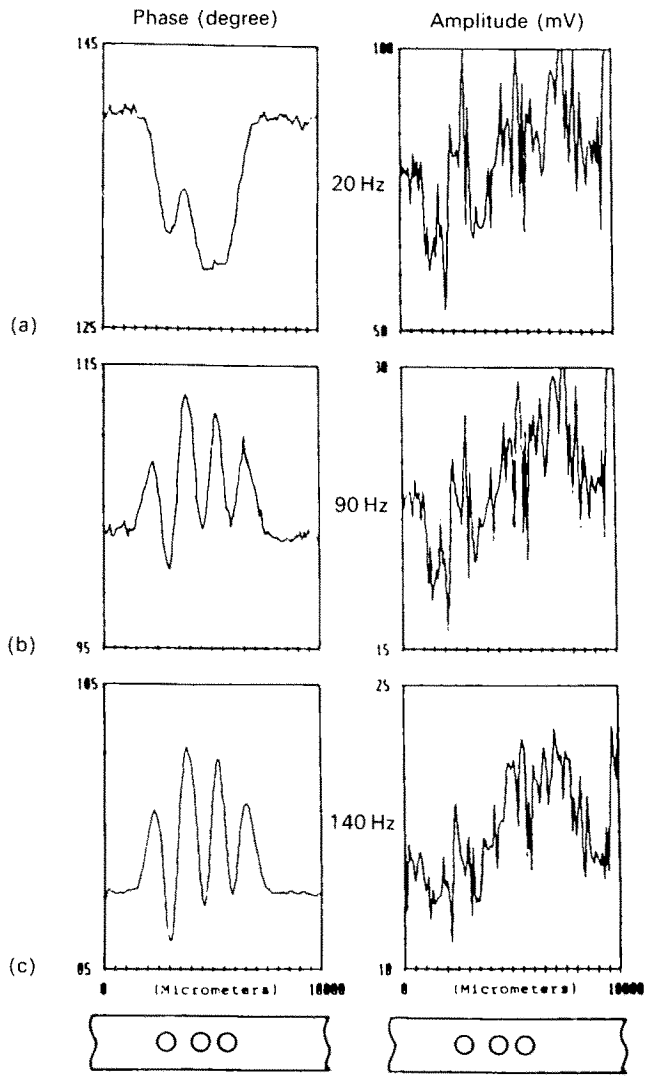

Figure 15 Example of a subsurface defect analysis demonstrated by the detection of holes of diameter 0.8 mm and separation 0.1 mm in a 3 mm thick aluminium plate, using different modulation frequencies: (a) 20 Hz, (b) 90 Hz and (c) 140 Hz.

For the characterization of extremely smooth surfaces, total integrated and angle-resolved scattering, stylus profilometry and heterodyne profilometry have been used. Scattering methods lead to statistical information about the surface and are contactless methods. By contrast, surface damage is risked with contacting-stylus profilometers. Heterodyne profilometers can give a height resolution of the order of 0.1 nm with a lateral resolution limited by diffraction to 1 μm. Care must be taken when the results obtained from different techniques are compared. Further investigations are needed because the results obtained using different techniques do not yet agree.

6. Application of fringe analysis together with computer-generated holograms

Computer-generated holograms are applicable for generating three-dimensional images from calculated holograms. They can be useful for optical filtering as well as for testing aspherical surfaces. Holographic optical elements (HOEs) are already used as beamsplitters and diffraction elements as well as deflection and focusing elements in laser scanners. HOEs are recorded by using plane and spherical waves as well as by means of computer-generated holograms.

The HOE is recorded by superposition of an object wave and a reference wave. The object wave can be reconstructed by illumination of the hologram after processing with a reconstruction wave similar to the reference wave.

The computer-generated hologram (CGH) is an exact analogy to the one recorded optically. The amplitude distribution in the hologram plane is calculated, the reference wave added, the sum squared and the result plotted. Sometimes this output needs to be photoreduced to provide a transparency for wave reconstruction. CGHs can be applied for testing aspherical surfaces with high precision. Testing aspherical surfaces together with fringe analysis is discussed below.

Aspherical optical surfaces are today being, and will be more frequently in the future, introduced into optical systems to improve the performance of optical systems and to reduce the number of optical elements, especially in image formation in the infrared. Recently aspherical single lenses were introduced to replace optical systems consisting of three or four elements in compact disc players.

Aspherical surfaces can be tested by a point-by-point analysis together with a three-dimensional measuring device to generate the surface profile. Interferometric methods, such as null test methods or shearing techniques, as well as the application of holographic techniques and CGHs are very useful for high-precision measurements [11].

CGHs can be used to compensate or compare complicated wavefronts for different applications. The CGH in a Twyman–Green experimental arrangement as shown in Fig. 16 can be used to compensate the aspherical wavefront reflected by the lens under test, for instance. Illuminating the CGH with the perfect aspherical wavefront computed from the optical data leads, after diffraction, to a perfect plane wave to be compared with the perfect reference plane wave from the reference beam reflected from mirror M. The interference fringes to be analysed are a measure of the discrepancy of the test lens from the data of the aspherical component or surface. Alternatively, an aspherical wavefront can be reconstructed from the CGH to be compared with the actual wavefront.

The principle of the CGH is not new. Wyant, among others, described the technique in optical shop testing [4]. Its application for the accurate, absolute test of steep aspherical surfaces as well as the generation of CGH needed to be improved.

For plotting CGHs a Calcomp plotter can be used, and different techniques have been devised or are in the process of being developed, such as the use of electron-beam scanners. We used a computer-driven Optronics drum scanner. A two-beam interference arrangement for an off-axis hologram for testing aspherical surfaces is shown in Fig. 16. The incident wave is separated by the beamsplitter into the reference beam reflected back from the mirror M slightly obliquely and passing through the hologram undisturbed and the test beam. For the fringe analysis one of the previously described techniques can be used. Because closed fringes need to be analysed, we prefer the phase-shifting technique with phase steps of $\pi/2$. The simple lenses L_1, L_2 and L_3 in Fig. 16 are auxiliary lenses to adapt the aperture

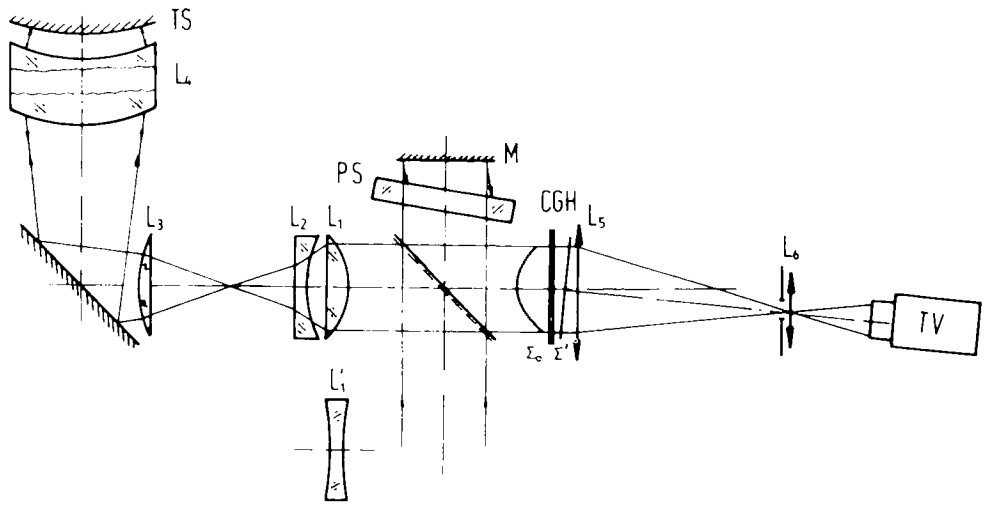

Figure 16 Arrangement for testing aspherical surface with a CGH. TS, surface to be tested; L_4, high-precision lens to be used for testing spherical and non-spherical lenses, L'_1 and L_4 produce a perfect spherical wavefront; L_1, L_2 and L_3, auxillary simple lenses to reduce the asphericity to a few hundred wavelengths as well as to adapt the aperture of TS; PS, plane-parallel plate for phase shifting; CGH, computer-generated hologram; M, mirror for the reference plane wave.

of the lens under test, TS. They should also image the test surface onto the CGH, a necessary condition for strong aspherical wavefronts. Furthermore, they can also be used to compensate partly the aspherical wavefront. L_4 is a high-quality lens to be used for testing aspherical as well as spherical lenses. In addition L_4 and L'_1 are used for focusing on the surface under test as well as for testing spherical surfaces with the same instrument. Furthermore, the accurate position of the vertex for spherical and aspherical surfaces is obtained with L'_1 in place, generating a perfect spherical wave.

Although the auxiliary lenses need not be perfect, a hologram is computed at first for a known spherical or aspherical surface for calibration purposes; the fringe analysis finally leads to a compensation of the errors involved which in turn are compensated when computing the CGH for the test surface.

Adjustment in an industrial test procedure can be time-consuming and difficult because seven degrees of freedom need to be balanced, such as tilt and decentring in two directions of the test surface as well as decentring and rotation of the hologram. Some of the adjustment errors have similar effects on the interference pattern.

Using the previously described automatic fringe analysis it was found appropriate to approximate the measured wavefront $W(r, \theta)$ by a set of polynomials. Zernike polynomials were frequently used because of their orthogonal properties. They lead to an elimination of the influence of the actual adjustment errors by matching the ray-tracing program and the measured wavefront [11].

7. Component and system analysis from interference patterns

Twyman–Green and Fizeau interference arrangements are frequently used for testing spherical and aspherical surfaces. By testing aspherical surfaces using CGHs for absolute measurement or for relative measurement using holographic techniques, the asphericity as

well as the adjustment errors of the test surface have to be determined. Adjustment errors can be evaluated from the interferogram and compensated. By testing aspherical surfaces the coefficients of asphericity and adjustment errors of the test surfaces and holograms can be determined from the interferograms. In a combined measuring procedure including ray tracing and fringe analysis, a procedure for system analysis was developed including the steps: automated fringe analysis; development of the measured wavefront of the fringe pattern into polynomials; considering polynomial coefficients as the goal for the optimization; and variation of the system parameters to obtain the best agreement between measurements and calculations.

For the procedure the wavefront will initially be determined by applying optical ray-tracing techniques leading to a fringe system. Usually a departure of the measured wavefront of the actual system from the computed occurs because the system parameters are slightly different.

The aim is therefore not so much the optimization of the original system, but the modification of the system parameters in such a way that the measured wavefront can be obtained in order to find the parameter errors in the system. Damped least-square techniques are useful. System parameters such as the radius of curvature and the refractive index centring errors are varied to obtain the measured wavefront. Zernike polynomials are very useful for system analysis. To compute the actual system starting with Zernike coefficients obtained from the fringe pattern, we can write

$$F_i = G_i(F_{ti} - F_{ai}) \tag{16}$$

where F_i are the Zernike coefficients obtained from the fringe pattern, G_i is a weighting factor and F_{ti} and F_{ai} are target and actual values, respectively. Writing Equation 16 in a Taylor expansion leads to

$$F_i = F_{0i} + \sum_{j=1}^{m} B_{ij}(x_j - x_{0j}) + \cdots \tag{17}$$

$B_{ij} = \delta F_i/\delta x_j$ is the sensitivity of the system by variation of parameters found from ray tracing. $x_j - x_{0j}$ can be found by inverting Equation 17. By variation of the parameter to approach the target x_j the deviation from the departure of the different system parameters from the theoretical values can be found.

Usually the number of equations is larger than the number of parameters. Therefore, the merit function should lead to a minimum.

Some of our applications of component and system analysis were the analysis of adjustment errors when testing spherical and aspherical surfaces, determination of the asphericity coefficients and vertex curvature of contact lenses; fine adjustments of air spacings in optical systems; and measurement of the refractive index of the elements of optical systems.

Adjustment errors occurring by the test procedure modify the fringe pattern. It should be noticed once more that by testing aspherical surfaces with CGH, seven degrees of freedom need to be considered. From the analysis of the fringe pattern the contribution of adjustment errors such as centring errors can be calculated and subtracted from the wavefront. By subtracting adjustment errors, included typically in some coefficients of the polynomials the surface errors should not be affected. A typical result of adjustment error subtraction from an interferogram is shown in Fig. 18, where an aspherical surface was tested with a CGH with adjustment errors introduced. Fig. 18a shows the fringe patterns with two additional centring errors of 0.02 and 0.2 mm introduced, and Fig. 18b represents the wavefront analysed with four different wavefronts with centring errors from 0.02 to

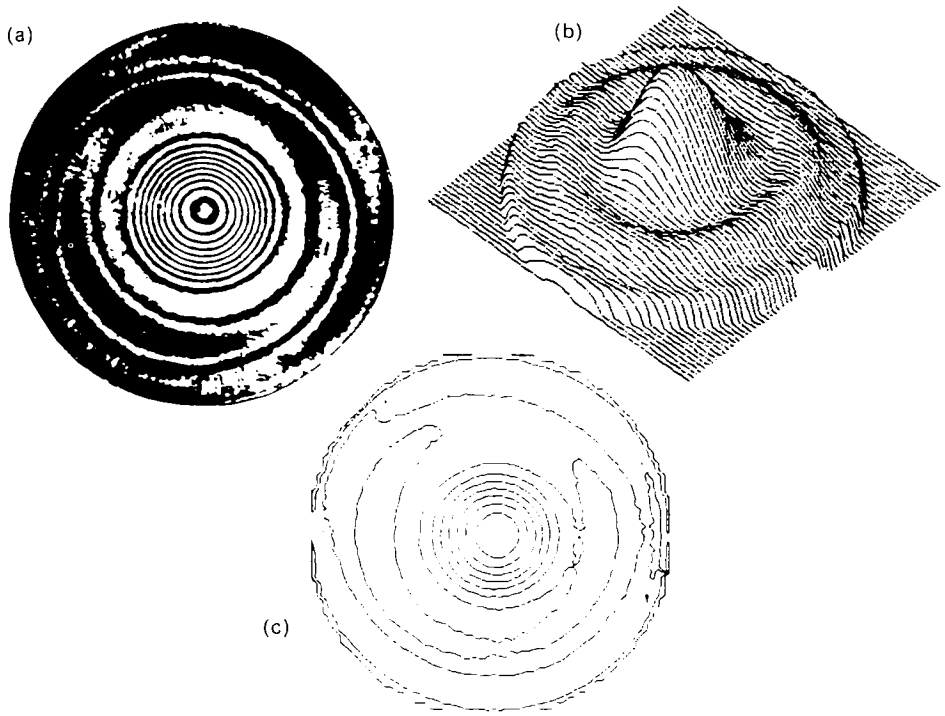

Figure 17 Results of a typical aspherical surface with high numerical aperture (NA = 0.6) tested with a CGH. (a) Fringe pattern, (b) pseudo-three-dimensional representation of the surface errors and (c) contour lines representing height deviation of 316 nm.

0.2 mm. The compensated wavefronts, without centring errors, are shown superposed in Fig. 18c, indicating the shape error only.

Contact lenses are frequently selected and specified by the vertex curvature and the asphericity parameter and the eccentricity of the back surface. The determination of such parameters from the fringe pattern is obtained with the procedure described in Equation 17. The measured wavefront can be described by Zernike polynomials. From the coefficients the vertex curvatures and asphericity coefficients are found by iteration, leading to the best fit of the measured fringe pattern.

8. Engineering application of holographic interferometry

Holography is a technique by which a wavefront of an object with an optically rough surface is recorded together with a reference wave. The reconstruction in the absence of the object leads to the same physical effect as the observation of the original object. Holographic interferometry enables the analysis of static and dynamic displacements of optically rough surfaces to be measured interferometrically. First reports of the method appeared in 1965 and were soon followed by numerous papers describing new applications [18, 19].

The major applications of holographic interferometry are in measuring mechanical displacement, vibration, stress and deformation. Depending on the application, different techniques were developed. Double-exposure, multiple- and time-averaged exposure techniques were introduced, as well as beam modulation and stroboscopic exposures [17, 18].

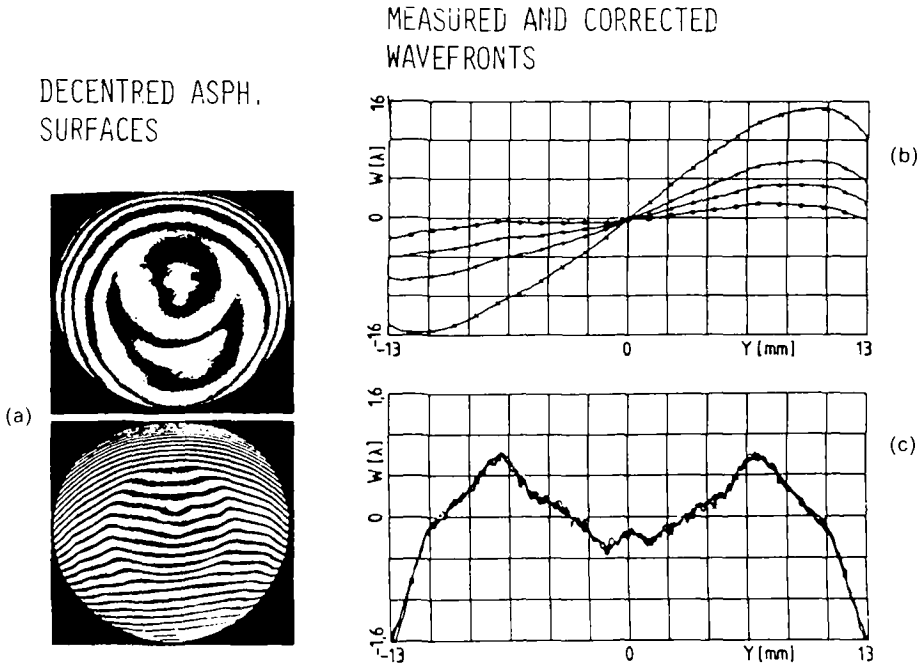

Figure 18 Adjustment error compensation from system analysis. (a) Fringe patterns with adjustment errors of the surface. (b) Wavefront of the surface with four different centring errors, the smallest and largest corresponding to the fringe patterns in (a). (c) Surface error with compensated centring errors.

In addition, fringe localizations together with fringe pattern analysis in three-dimensional space have been investigated. By 1970 published material was available predicting the object motion from the fringe pattern. Methods were established to extract vectorial object displacement from the fringes, their parallax and their localization required in their applications. The search for simpler techniques of fringe analysis in holographic interferometry initiated various studies [20]. The theories developed so far simplify the analysis and make it easier for the engineer to understand and apply it. Sometimes, however, they are too difficult to be of practical value for three-dimensional engineering problems, but they can be very useful for special applications.

In recent years matrix methods and tensor calculus [18] have been introduced for fringe analysis, leading to a number of strain analysis techniques. Phase detection has been significantly improved to one part in 100 or even 1000 by phase measuring and heterodyne interferometry [1]. Now, at last, holographic interferometry is beginning to show its true potential in structural metrology.

9. Holographic interferometry for rotating objects

Holographic interferometry can be useful for deformation and stress analysis, as well as for the study of vibrations. Contour-line holography with automatic fringe analysis can lead to a powerful tool for engineering applications.

The analysis of deformation, stress and vibration of rotating objects will be discussed further. It requires unwanted rigid-body rotation to be eliminated while preserving the

information about the elastic object deformation. Three methods could be used to carry out holographic interferometry and speckle techniques on rotating objects. These are stroboscopic, rotating plate and image-derotated holographic interferometry.

The stroboscopic method consists of making a hologram of the object while it is stationary. For the second exposure with strobed light, the rotating object is illuminated, the illumination being at the same angular orientation to the object as for the first exposure.

Rotating-plate holographic interferometry uses a holographic plate fixed to the rotating axis of the object, but this is not always possible. In addition, the rotating hologram itself will be subjected to vibration or rigid-body motion, so complicated fringe analysis results.

Image derotation [21] is the most promising approach for the study of rotating objects with holographic or speckle techniques. In this method the image of the rotating object is passed through, or reflected by, a prism rotating at half the rotational speed of the object, thus cancelling the rotational motion. A Q-switched double-pulse ruby laser is then used to produce a double-exposure hologram of the rotating object [15].

The experimental set-up used for image-derotated holographic interferometry is shown in Fig. 19. Light from the double-pulse ruby laser is divided by a beamsplitter and illuminates the object via a second beamsplitter. The reflection of the object passes through the derotator prism to interfere with the reference beam on the holographic plate and forms an image-plane hologram. For the alignment it is important that the axis of the derotator is collinear with the rotational axis of the object, otherwise optical path length differences will produce bias fringes between the two laser pulses. The exact 2 : 1 ratio between the

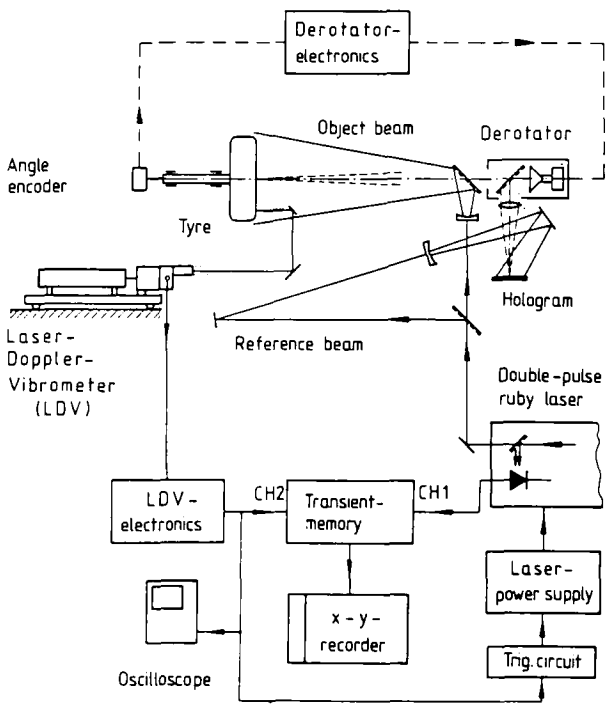

Figure 19 Arrangement for double-pulse holography with an image derotator for the vibration analysis of a rotating car tyre. The derotator prism rotates at half the speed of the tyre, controlled by the angle decoder.

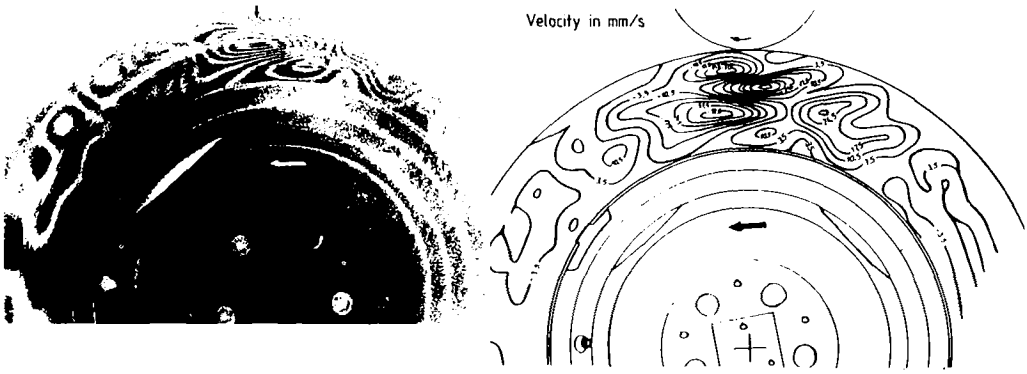

(a) (b)

Figure 20 Example of the double-pulse holography for the vibration analysis of the side wall of a rotating car tyre. (a) Fringe pattern by simulated road contact with $n = 320\,\text{min}^{-1}$ and pulse width separation of 40 ns and pulse separation 100 μs. (b) Contour lines of constant amplitudes of (a).

object and prism speed is achieved by mounting an encoder disc on the drive shaft of the object and relaying its signals to an electronic unit controlling the speed of the servo-motor.

In a research project we have studied the noise of rotating car tyres. Fig. 19 shows the experimental arrangement with a derotator and double-pulse ruby laser. Fig. 20a shows the fringe pattern obtained by pulse separations of 100 μs at $n = 320\,\text{min}^{-1}$ and a pulsewidth of 40 ns, and Fig. 20b shows the lines of equal velocity.

For noise analysis a frequency analysis of the vibration as described previously is required. A heterodyne technique can be used for the analysis of the amplitude and for the frequency of vibration at one or several points. This also facilitates fringe analysis of holographic interferometry. The two methods can therefore be used in parallel, the heterodyne technique for the analysis of the vibrations at a given point and the holographic for the analysis of the spatial amplitude distribution of the vibration with reference to the movements at a single point (Fig. 12).

10. Holographic interferometry in quasi-real-time

The storage media used for holographic interferometry are mainly photographic materials based on silver halide. Alternatives are photoresists, dichromated gelatine, photochromic or thermoplastic materials, or photorefractive electro-optical crystals. Thermoplastic storage material is frequency used in holographic interferometry.

Holographic interferometry is more attractive to the engineer when it can be applied in real time. Photofractive materials such as lithium niobate ($LiNbO_3$), potassium niobate ($KNbO_3$), barium titanate ($BaTiO_3$), strontium barium niobate (SBN) and bismuth silicon oxide ($Bi_{12}SiO_{20}$) are attractive new candidates for real-time optical data-processing. Reversible holographic storage was first demonstrated in $LiNbO_3$. More recently, $BaTiO_3$, and $Bi_{12}SiO_{20}$ (BSO) and $Bi_{12}GeO_{20}$ (BGO) were applied for the storage of holograms and speckle patterns [22, 23]. Photorefractive crystals can be used for real-time metrology using holography in a two- or four-wave mixing arrangement. We very often use BSO crystals in our laboratory because BSO is known to be a relatively fast and sensitive material, with a

relatively small electro-optic coefficient. By contrast, $BaTiO_3$ has larger electro-optic coefficients and is highly efficient, but responds slowly.

One model to describe the charge transport in the photorefractive material is the band transport model assuming that electrons (or holes) are optically excited from filled donor (or acceptor) sites to the conduction (or valence) band where they migrate to dark region in the crystal by drift or diffusion before recombining into an empty trap. The transported charges result in an ionic space-charge grating which is, in general, out of phase with the incident irradiance. The space charge grating is balanced by a periodic space-charge electric field modulating the refractive index through the electro-optic effect. The sensitivity of the BSO is comparable with that of the Kodak 649 F emulsion (0.3 mJ cm $^{-2}$) and the information (hologram) can be stored for more than 24 h. Flooding with uniform illumination leads to erasure of the stored information by space-charge relaxation. Consequently, reading out with the recording wavelength is destructive.

For holographic interferometry in quasi-real-time one hologram of the object to be studied is stored in the crystal as shown in Fig. 21. Shortly after the deformation has taken place, a second hologram is stored and reconstructed together with the first one. Interference fringes occurring in quasi-real time are a measure of the wavefront deformation between the first and the second exposure. For the analysis of the fringe pattern, TV techniques as described are useful. For harmonically oscillating objects, holograms can be recorded while the object is oscillating. By reconstructing the stored time-averaged hologram the vibration amplitude can be analysed.

For contour-line holography in quasi-real time a BSO crystal can be used as storage material [22]. There are different ways to form contour fringes that are contours of constant range of depth. The object can be illuminated with two wavelengths simultaneously, illuminated with one wavelength but from two directions, or with one wavelength but with a medium of different index surrounding the object (to be changed between exposures).

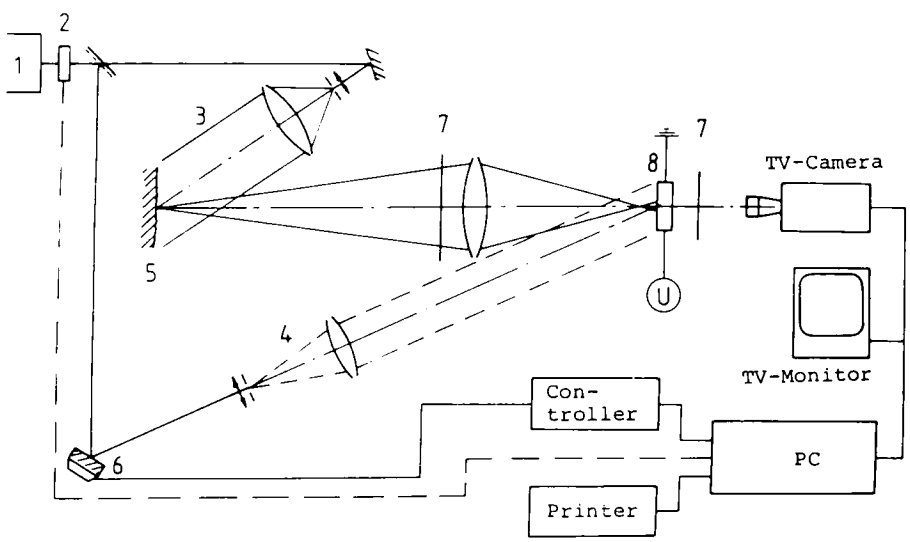

Figure 21 Arrangement for quasi-real-time holography using a photorefractive crystal as storage material. 1, Argon laser; 2, shutter; 3, object beam; 4, reference beam; 5, object; 6, piezo-driven mirror; 7, polarizer; 8, BSO crystal.

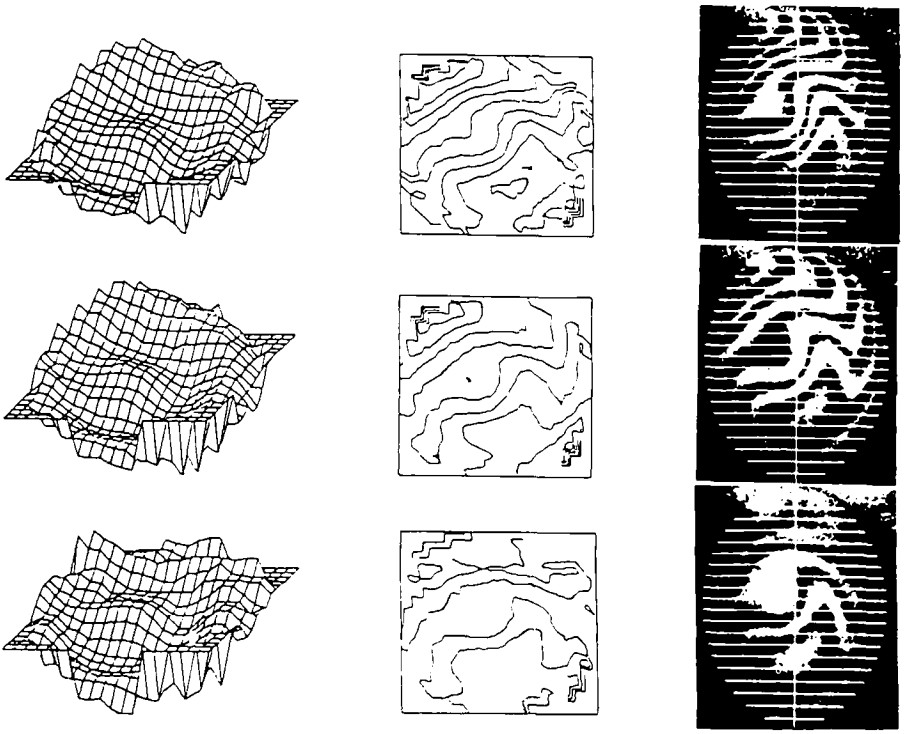

Figure 22 Deformation of a two-component glue by curing taken in intervals of 30 s. (a) Fringe pattern photographed from TV screen, (b) contour lines and (c) pseudo-three-dimensional representation.

An application of quasi-real-time holographic deformation measurement will be discussed briefly. To study the curing glue, double-exposure holograms were recorded using the experimental set-up shown schematically in Fig. 21. Immediately after the second exposure the hologram is reconstructed and analysed using the phase-shifting technique described above, by moving a mirror in the reference beam. After using a flash the crystal is ready for the next exposure. In Fig. 22 typical fringe patterns photographed from the TV screen taken in intervals of 30 s are shown, together with contour lines and pseudo-three-dimensional plots.

11. Application of speckle techniques in metrology

When an optically rough surface is illuminated by a laser a speckle phenomenon occurs; it is a curious granular appearance. A similar effect occurs in coherent radar and ultrasonic imaging. By an optical rough surface we mean height variations of the order of, or greater than, the wavelength of the illuminating light. When such a surface is illuminated by a laser beam the intensity of the scattered light is found to vary randomly with position.

When a laser-illuminated optically rough object undergoes displacement and/or deformation, the speckles in the image field of the object move in the same way but are accompanied by a change in the structure by larger displacements.

11.1. Speckle photography

Speckle techniques are useful tools for determining displacements, vibrations, deformations and contours of a wide range of optically rough surfaces [24]. In speckle photography an optically rough surface is illuminated with coherent light and photographed in the image plane, the Fourier plane or a defocused plane, depending on the application. The recorded image will have a speckled appearance. Exposing the image on photographic film or BSO before and after a small object movement (double exposure), pairs of practically identical speckles are recorded. Illuminating the developed double-exposed speckle pattern with a laser beam, Young's fringes are obtained in the Fraunhofer diffraction plane, with a separation inversely proportional to the object displacement. Young's interference fringes occur only if the displaced speckles remain correlated. A point-by-point analysis of the in-plane motion of the displacement vector field can be carried out even in the presence of small out-of-plane movements. In Fig. 23 Young's fringe of speckle patterns recorded before and after bending a lever are shown. The fringe separation is inversely proportional to the bending.

Speckle photography is by now understood well and can be an useful tool in optical metrology. The limitations are those due to strong deformations (strain), rotation and tilt. For example, deformation and tilt in the presence of translations lead to a limitation of speckle photography due to loss of speckle correlation [24].

By measurements of the spacing and the orientation of the Young's fringe patterns for points on a square-mesh lattice, the two-dimensional strain field can be evaluated. Visual methods for the fringe analysis are time-consuming and limited to small sample regions, and are heavily dependent on the skill of the operator. For these reasons electro-optical

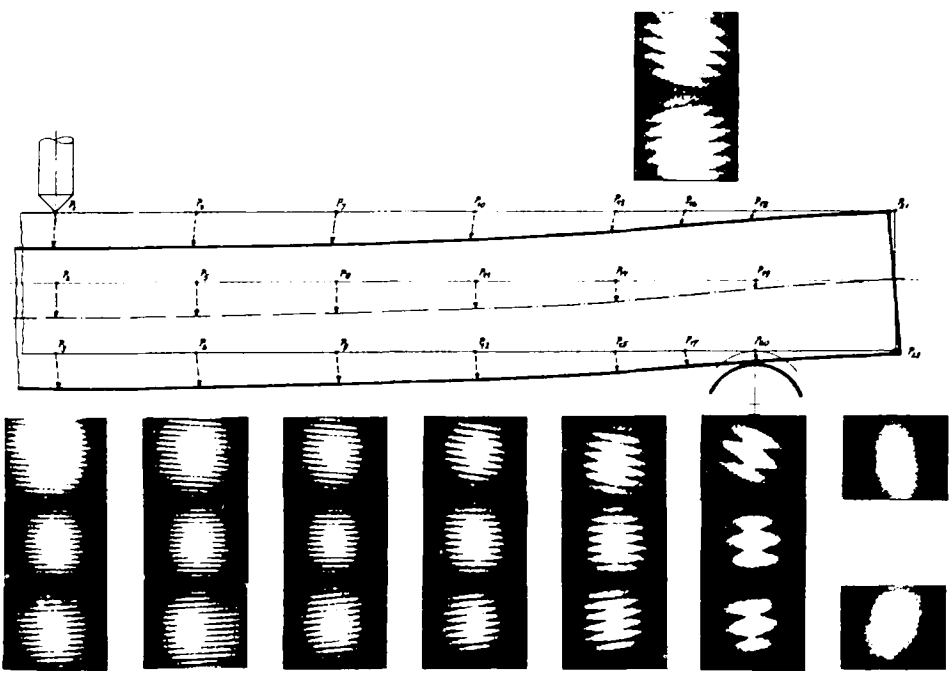

Figure 23 Measurement of the deformation of a lever using speckle photography.

read-out systems and automatic fringe analysis have been studied recently. For fringes with good contrast, speckle displacements were obtained down to 0.1 μm standard deviation.

Bruhn and Felske [25] developed a fast, two-dimensional Fourier transform analysis of Young's fringes using TV techniques together with image analysis methods in order to construct an automatic fringe analysis system.

11.2. Electronic speckle-pattern interferometric system

For recording the interference pattern of diffusely reflecting objects, different names are found in the literature, namely electronic speckle pattern interferometry (ESPI), TV speckle interferometry [19] and TV holography [24–28]. ESPI can be described similarly to a holographic method. A specular reference beam as in conventional holography is usually superimposed on the speckled object beam into a camera. For a moving object the intensity in the speckles varies cyclically, corresponding to a path-length change between reference and object beam by λ, for instance (λ being the wavelength of the laser). The video signal is processed, high-pass filtered, rectified and displayed on the TV monitor. The electronic processing can be considered to correspond to the reconstruction in conventional holography where the interference fringe pattern needs to be stored, requiring high resolution. In speckle interferometry, however, the resolution of the storage device needs to be adapted to the speckle size which can, in turn, be adjusted by the aperture of the image-forming lens.

For deformation, displacement or vibration analysis, speckle interferograms of different states are added or subtracted. The subtraction of speckle patterns is discussed below.

11.3. Speckle pattern correlation fringe formation by video signal subtraction

By the superposition of a speckle field and a reference wave, the intensity in the detector plane can be written as

$$I = I_0(1 + b\cos\phi) \tag{18}$$

where $I_0 = I_R + I_S$, I_R and I_S being the intensity in the detector plane of the reference and speckle field, respectively, and $b = 2(I_R I_S)^{1/2}/I_0$. After a small displacement of the object, the phase ϕ changes into $\phi + \Delta\phi$. Assuming that the output signal of the detector is proportional to the intensity, we obtain the detector signal, by subtracting the signal after deformation or displacement from the original

$$\begin{aligned} U_S &= b[\cos\phi - \cos(\phi + \Delta\phi)] \\ &= 2b\sin\left(\phi + \frac{\Delta\phi}{2}\right)\sin\left(\frac{\Delta\phi}{2}\right) \end{aligned} \tag{19}$$

The signal can be rectified and the brightness averaged along a line of constant $\Delta\phi$. The fringe pattern obtained leads to a maximum for $\Delta\phi = (2m + 1)\pi$ and a minimum for $\Delta\phi = 2m\pi$; $m = 0, 1, 2, 3, \ldots$. On the monitor, fringe patterns occur for $\Delta\phi = (2m + 1)\pi$, depending on the phase difference due to the object motion between the two states of the recording.

Fig. 24 show schematically the experimental set-up used. The speckled object wavefront and the reference are superimposed and imaged onto the CCD camera, stored and subtracted. Furthermore, for the fringe analysis a piezo driven mirror (PZT) is introduced into the reference beam to shift the phase in steps as described earlier. The reference is introduced by means of a monomode fibre. A typical fringe pattern is shown in Fig. 25a. It should be

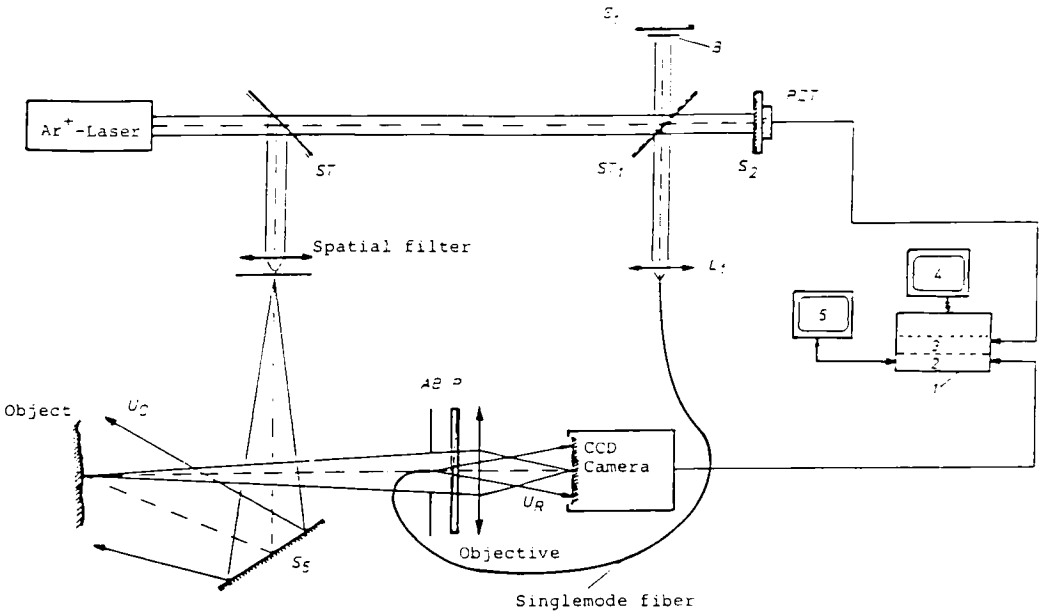

Figure 24 Arrangement with phase shifting for speckle interferometry. 1, PC; 2, digital image storage; 3, digital-to-analogue converter; 4, monitor; 5, TV monitor; S_2, mirror with PZT for phase shifting.

noted that some filter operations such as averaging and convolution are needed to clean the speckled fringe pattern. In Fig. 25b and c contour lines of deformation with a depth variation of 0.81 μm and a pseudo-three-dimensional presentation of the deformation are shown.

Speckle interferometry can become a powerful tool for engineering applications, especially when it can be applied in 'real time'. When movements parallel to the line of sight need to be measured, the lateral speckle shift should be smaller than the mean speckle size. For in-plane strain measurement the object can be illuminated obliquely with two plane waves [24].

12. Moiré techniques for industrial inspection

Moiré techniques extend the range of holographic and speckle interferometry for out-of-plane and in-plane displacement, and for deformation measurements and topography. Moiré patterns can be formed by many types of gratings. In this review we restrict ourselves to the Moiré contouring using shadow-Moiré techniques with projected gratings. Further applications of the Moiré techniques are described in [30].

A Moiré pattern consists of light and dark fringes-like lines of equal surface heights or change in surface position. It is obtained by producing a grating-like structure on the object by projecting either a grid or an interference pattern, as will be described briefly. Height variations or deformations lead to a deformation of the projected fringes, which in turn compared with the original or synthetic grating like structure leads to the Moiré fringes [29, 30]. Typical contour-line separations are of the order of or greater than a fraction of a millimetre. Moiré techniques can also be used for microsurface analysis.

Fig. 26 shows an arrangement we used at our institute. The fringes are produced by a relative tilt between mirrors M_1 and M_2 and a line structure that can be adapted

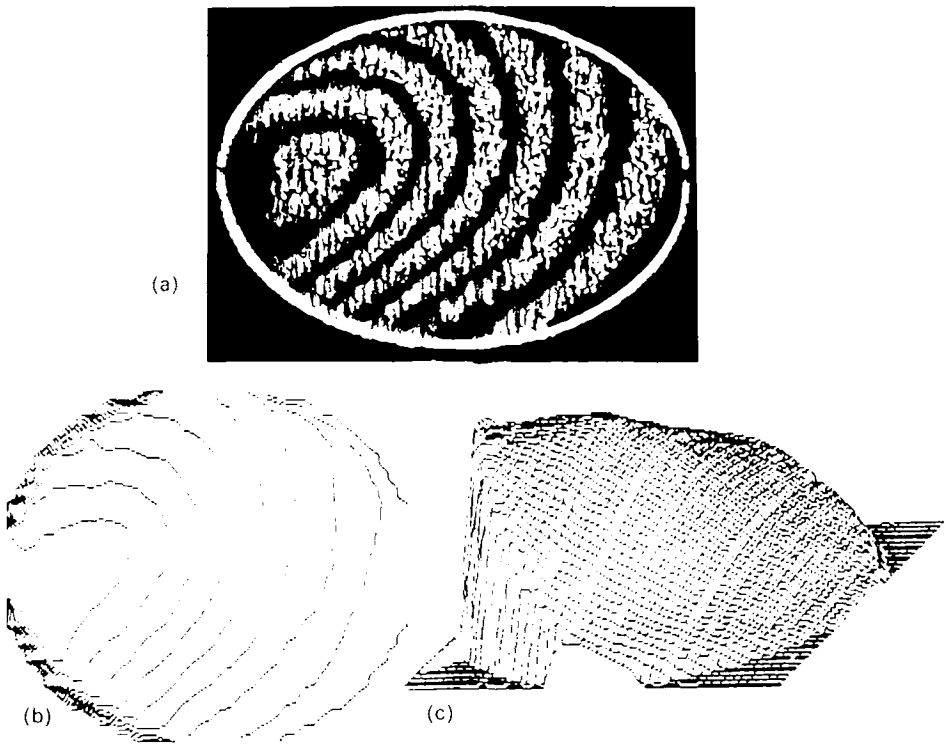

Figure 25 Fringe analysis in speckle pattern interferometry. (a) Speckle pattern obtained by subtraction. (b) Contour lines of equal deformation with $\Delta h = 0.81\ \mu m$. (c) Pseudo-three-dimensional representation of the deformation.

depending on the application by tilting the mirror M_1. Furthermore, for the analysis of steps, two different grating periods or structured illumination are needed. A piezo-element is used to shift the phase for the analysis of the Moiré fringes using one of the phase-stepping techniques described. By changing the phase, the fringes on the object will move in steps of, say, one-quarter of the period. A typical application is shown in Fig. 27a, where a contour map of the mount of an electric light bulb with a contour-line spacing corresponding to Δz of 1 mm is presented. Fig. 27b shows the pseudo-three-dimensional representation of the bulb mount with a peak to valley distance, PV, of 32.9 mm. The time necessary for the fringe analysis was 10 s.

A number of techniques have been developed, the choice of an appropriate technique depends on the sensitivity required, which in turn can be adjusted. Moiré techniques are not as sensitive as holographic techniques. The sensitivity of the Moiré technique can be adapted to the requirements by selecting the appropriate fringe spacing of the grading projected onto the object, an adaption hardly possible in holography. Furthermore, the technique is less sensitive to disturbances, such as vibration and positioning, than is holography.

Real-time Moiré techniques are useful for detecting vibration patterns and identifying the kind of motions present. Probably the widest application of Moiré techniques is in the field of measurement for industrial applications where changes are larger than typically studied

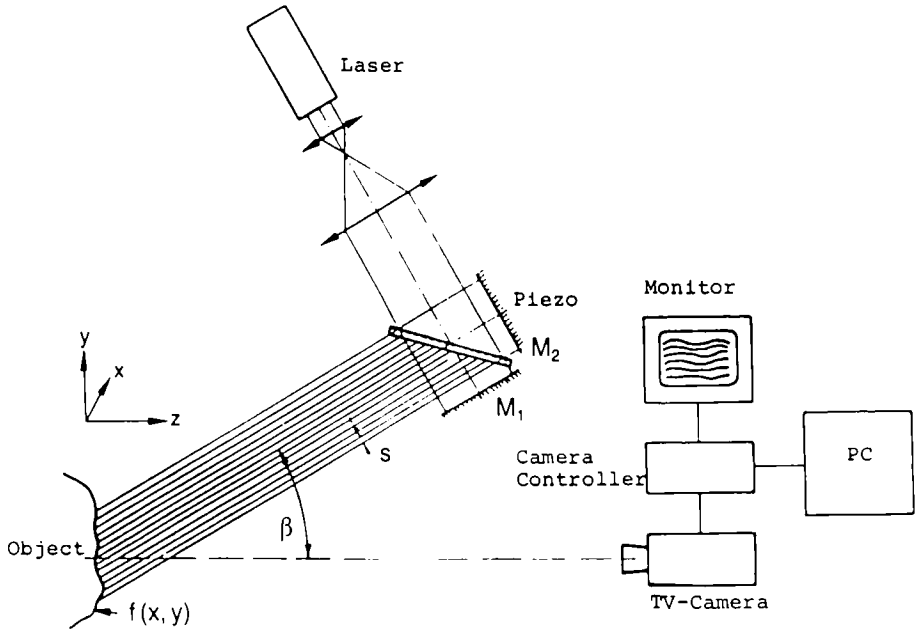

Figure 26 Moiré arrangement with the grating period to be adapted by tilting the mirror M_1. M_2 is shifted by a piezo for fringe analysis.

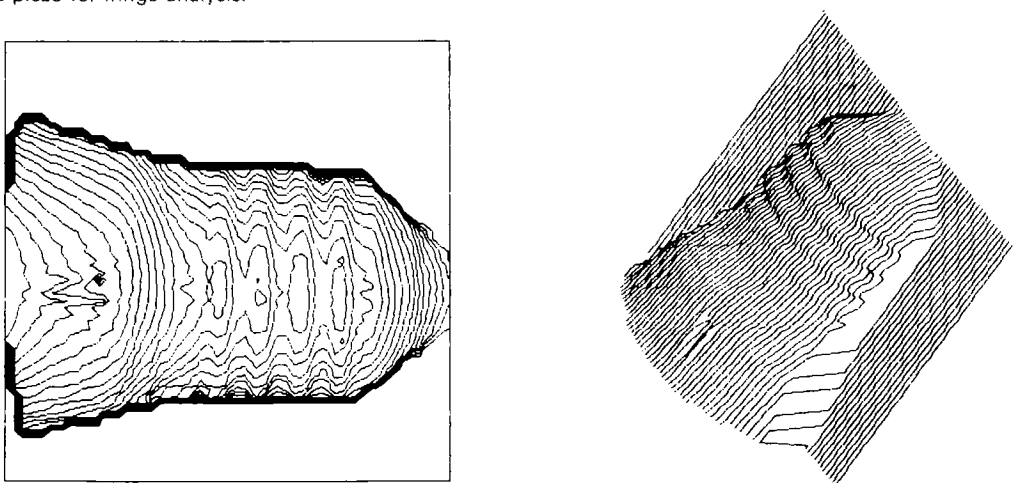

Figure 27 (a) Contour map of a mount of an electric bulb with contour lines corresponding to Δz = 1 mm. (b) Pseudo-three-dimensional representation of (a) with peak to valley distance, PV, of 32.9 mm.

with holographic interferometry. The Moiré techniques can be used to complement interferometric, holographic and speckle techniques, and therefore to expand the arsenal of capabilities of optical non-destructive testing.

13. Conclusion

Progress has been made in the fringe analysis procedure. At last interferometric, holographic, speckle and Moiré techniques can be applied more frequently in industry. Optical methods

can also be very useful for micro- and macrostructure analysis in a production process. Further work is needed to make optical methods more reliable, even in a rough environment. In addition, optical precision measuring methods will be more frequently applied in the production process of microelectronics.

References

1. R. DÄNDLIKER, in 'Progress in Optics', Vol. XVII, edited by E. Wolf (North-Holland, Amsterdam, 1980) p. 1.
2. M. TAKEDA, H. INA and S. KOBAYASHI, *J. Opt. Soc. Am.* **72** (1982) 156.
3. TH. KREIS, *J. Opt. Soc. Am.* **A3** (1986) 847.
4. J. H. BRUNNING, in 'Optical Shop Testing', edited by D. Malacara (Wiley, New York, 1978) 409.
5. B. DÖRBAND, *Optik* **60** (1982) 161.
6. J. SCHWIDER, R. BUROW, K. E. ELSNER, J. GRZONNA, R. SPOLACZYK and K. MERKEL, *Appl. Opt.* **22** (1983) 3421.
7. J. C. WYANT, C. L. KOLIOPOULOS and B. BUSHBAN, *ASCE Trans.* **27** (1984) 101.
8. K. CREATH, *Proc. SPIE* **680** (1986).
9. F. M. KÜCHEL, TH. SCHMIEDER and H. J. TIZIANI, *Optik* **65**, (1983) 123.
10. H. J. TIZIANI, in 'Rechnerunterstützte Laser-Meßtechnik', Technisches Messen, Vol. 54 (1987) 221.
11. B. DÖRBAND and H. J. TIZIANI, *Appl. Opt.* **24** (1985) 2604.
12. C. C. HUANG, *Opt. Engng* **23** (1984) 365.
13. S. E. GREIVENKAMP, *ibid.* **23** (1984) 350.
14. K. LEONHARDT, K.-H. RIPPERT and H. J. TIZIANI, in 'Optische Profilometrie und Rauheitsmessung', Technisches Messen, Vol. 54 (1987) 243.
15. U. ESSERS, R. EBERSPÄCHER, W. LIEDL, R. LITSCHEL, B. PFISTER, H. J. TIZIANI and A. ZELLLER, 'Entwicklungslinien in Kraftfahrzeugtechnik und Straßenverkehr' (Verlag TÜV Rheinland, Köln, 1981).
16. G. BUSSE, *IEEE Trans. Sonics Ultrasonics* **SU-32** (1985) 355.
17. Z. SODNIK and H. J. TIZIANI, *Opt. Commun.* **58** (1986) 295.
18. W. SCHUMANN and M. DUBOIS, 'Holographic Interferometry', Springer Series in Optical Science, Vol. 16 (Springer-Verlag, Berlin, 1975).
19. R. JONES and C. WYKES, 'Holographic and Speckle Interferometry' (Cambridge University Press, 1983).
20. B. BREUCKMANN and W. THIEME, *Appl. Opt.* **24** (1985) 2145.
21. W. F. FAGAN, M. A. BEECK and H. KREITLOW, *SPIE Proc.* **36** (1980) 260.
22. H. J. TIZIANI, *Optica Acta* **29** (1982) 463.
23. J. P. HUIGNARD, J. P. HERRIAU, P. AUBOURG and E. SPITZ, *Opt. Lett.* **4** (1979) 21.
24. R. K. ERF, (editor), 'Speckle Metrology' (Academic Press, New York, 1978).
25. H. BRUHN and A. FELSKE, *VDI Ber.* **309** (1981) 13.
26. K. CREATH, *Appl. Opt.* **24** (1985) 3053.
27. S. NAKADATE, *ibid.* **25** (1986) 162.
28. E. FISCHER, Studienarbeit, ITO, Universität Stuttgart (1986).
29. K. J. GASVIK, 'Optical Metrology' (Wiley, New York, 1987).
30. L. PIRODDA, *Opt. Engng* **21** (1982) 640.